**NATIONAL TECHNICAL UNIVERSITY OF ATHENS**
**SCHOOL OF ELECTRICAL AND COMPUTER ENGINEERING**
**SCHOOL OF MECHANICAL ENGINEERING**

INTERDISCIPLINARY POSTGRADUATE PROGRAMME

Translational Engineering in Health and Medicine (TEAM)

---

# Modelling Long Term Human Brain Activity: Are models still valid given errors in measurement?

---

Postgraduate Diploma Thesis

Kontessa Ioanna Zorpala

Supervisor

Prof. Konstantina Nikita
Professor in School of Electrical and Computer Engineering
National Technical University of Athens

Co-Supervisor

Prof. Marcus Kaiser
Professor of Neuroinformatics, School of Medicine
University of Nottingham

Athens, October 2024

**NATIONAL TECHNICAL UNIVERSITY OF ATHENS**
**SCHOOL OF ELECTRICAL AND COMPUTER ENGINEERING**
**SCHOOL OF MECHANICAL ENGINEERING**

INTERDISCIPLINARY POSTGRADUATE PROGRAMME
"Translational Engineering in Health and Medicine"

---

# Modelling Long Term Human Brain Activity: Are models still valid given errors in measurement?

---

Postgraduate Diploma Thesis

Kontessa Ioanna Zorpala

Supervisor
Prof. Konstantina Nikita
Professor in School of Electrical and Computer Engineering
National Technical University of Athens

Co-Supervisor
Prof. Marcus Kaiser
Professor of Neuroinformatics, School of Medicine
University of Nottingham

The postgraduate diploma thesis has been approved by the examination committee on October 14th, 2024

| *1st member* | *2nd member* | *3rd member* |
|---|---|---|
| **Dr. Konstantina S. Nikita** | **Dr. Marcus Kaiser** | **Dr. Athanasios Voulodimos** |
| *(Prof. in NTUA)* | *(Prof. in the University of Nottingham)* | *(Assistant Prof. In NTUA)* |

Athens, October 2024

**Kontessa Ioanna Zorpala**
Graduate of the Interdisciplinary Postgraduate Programme,
"Translational Engineering in Health & Medicine",
Master of Science (MSc),
School of Electrical and Computer Engineering,
National Technical University of Athens

# *Abstract*

**Whole Brain Emulation (WBE)** represents one of the most ambitious objectives in contemporary computational neuroscience, aiming to replicate human brain activity within a computational model. This study investigates the role of measurement errors during the data acquisition phase and their subsequent impact on neural simulations, focusing on the Kuramoto and Izhikevich models. Both models were employed to simulate the dynamics of different brain regions, particularly focusing on the introduction of noise that mimics errors originating from brain imaging techniques.

Our analysis begins with the observation of how noise affects neural dynamics by segmenting the simulations into three phases: (1) the control phase before noise introduction, representing a brain's natural state; (2) the branching point, where noise is introduced as a representation of data acquisition errors in WBE; and (3) the simulation of both control data (undisturbed brain function) and noisy data (the behavior of a brain replica impacted by measurement errors).

A key finding of this work is the clear correlation between noise levels and the total error in both models, confirming that higher noise results in greater error. This underscores the critical importance of using precise measurement techniques during the data acquisition phase and suggests the need for developing error-correction mechanisms to mitigate the impact of noise. We also investigated the impact of connectivity strength in specific brain regions, revealing distinct differences between the models. In the Kuramoto model, regions with higher connectivity contributed more to the final error, while in the Izhikevich model, these same regions tended to reduce error as their connectivity increased.

These findings are significant because they highlight the need for further investigation into measurement error in WBE, in addition to ongoing work on computational and hardware aspects of brain emulation. As demonstrated, noise introduced by data acquisition has a profound impact on neural simulation accuracy, and addressing this challenge is essential for achieving reliable WBE. Additionally, while the models employed in this study lack certain biological realism, including synaptic plasticity and adaptive behavior, they still offer valuable insights into how noise and learning mechanisms may influence neural dynamics in computational models. This work lays the foundation for future research aimed at improving both the fidelity of neural simulations and the accuracy of data acquisition techniques.

***Keywords**: Whole Brain Emulation, Measurement Error, Neural Simulation, Connectome*

# *Acknowledgements*

I would like to express my sincere gratitude to Professor Marcus Kaiser, who guided, encouraged, and mentored me throughout this insightful project. His support and expertise have been invaluable.
I am also deeply grateful to the Captain Fanourakis Foundation (CFF) for their generous support, which enabled me to fully focus on my research and academic endeavors.
To my family, the friends I already had, and the ones I made along the way, thank you for your unwavering encouragement.

# Contents

# List of Figures

# Chapter 1

# Introduction

Chapter 1. *Introduction*

## 1.1 Background

The brain, often described as the human black-box, due to its opacity and complexity, is responsible for myriad cognitive and survival processes, and therefore, has been the focus of extensive research for many years. **Computational neuroscience**, leverages the methods and benefits of computers, to describe how the brain uses electrical and chemical signals to represent and interpret both external and internal information [1]. This objective has remained unchanged through the years. Moreover, advancements in neuroimaging techniques and the increased availability of computing power, nowadays, allow realistic simulations of neural systems, enabling modelling large numbers of neurons with greater accuracy.
Studying long-term brain activity is crucial for advancing our knowledge in neuroscience, developing treatments for neurological disorders and achieving the ultimate ambitious goal of brain emulation.
**Whole Brain Emulation (WBE)** is a concept which includes a computational model to replicate the functions and consciousness of the human brain [2]. This is achieved through thorough scanning and mapping an actual biological brain's structure and connectivity, followed by simulating this complex configuration on a high powered computer system. The feasibility of WBE is based on the theory of *Computationalism in the philosophy of mind*, which proposes that each mental state corresponds to a computational state [3]. Therefore, a clear credence to the possibility

of recreating human cognitive processes through computation is created. This process involves several steps:

1. **Brain Scanning:** High detailed imaging of the brain's structure, down to the level of individual neurons and their connections (synapses).
2. **Data processing:** Converting the scanned data into a format that a computer can understand and manipulate, effectively creating a **connectome**, which is a comprehensive map of neural connections [4].
3. **Simulation:** Running the processed data on a computer to emulate the brain's function, thereby recreating the individual's cognitive processes, including memory, personality and consciousness.
4. **Validation & Testing:** Once the simulation is complete, it is vital to assess the model's accuracy and sufficiency in replicating the brain's functionalities. Thus, multiple comparisons between responses of the emulated brain to that of the biological brain under identical conditions takes place, through rigorous testing of either known cognitive functions, such as memory recall or problem solving abilities (direct testing), or evaluations of the model's ability to simulate brain-pattern activities, such as neural oscillations (indirect testing) [5].

## 1.2 Motivation of this Study

While WBE opens up new prospects on achieving human-level artificial intelligence potentially expanding human consciousness into digital realms, several powerful obstacles have yet to be overcome. WBE begins with the critical step of brain scanning. This process involves capturing highly detailed images of the brain's structure, including individual neurons and their intricate connections. Despite the advancements in the field of medical imaging, a persistent challenge of this domain is the presence of noise generated during data acquisition. These so-called **measurement errors** can arise from various sources such

as limitations in imaging resolution, variability in imaging conditions, and technical imperfections in the equipment used.
Given that brain scanning serves as the foundation for subsequent data processing, modelling and simulation, any errors introduced at this stage can propagate through the entire workflow, potentially compromising the accuracy and validity of the brain models. Therefore, shedding light to the way these initial measurement errors impact the overall fidelity of brain simulations, is imperative. By examining the effects of these errors, this project aims to assess the robustness and reliability of current brain modelling techniques.
Accurate brain emulation has the potential to revolutionize various fields, including neuroscience and artificial intelligence, by providing more thorough insights into brain function and dysfunction. It could aid in the development of new therapies for neurological disorders, improve brain-computer interfaces (BCIs), and even contribute to advancements in cognitive augmentation and enhancement technologies. The ripple effects of improving brain model accuracy extend far beyond academic research, influencing practical applications that can significantly impact human health and technological progress.
The motivation behind this study, is not only to quantify the impact of measurement errors but also provide insights that could lead to more robust brain modelling practices. By doing so, we aim to contribute to the ongoing efforts in neuroscience to create accurate and functional simulations of the human brain, ultimately moving closer to the goal of WBE.

## 1.3 Research Questions

This study aims to address several questions regarding the reliability and validity of brain modelling techniques and the influence of measurement errors during the brain scanning process. Since WBE relies heavily on neural connection mapping, even small errors captured during the imaging process, via resolution limitations and technical imperfections, can result in incorrect data representation. Understanding how these measurement inaccuracies propagate through the modelling process is vital for

evaluating these models' reliability.
Furthermore, a key aspect of this project is examining whether the brain's inherent neural properties, such as learning and plasticity, could help in minimizing or even restoring the effects of the initial measurement errors. Neural plasticity, the capacity of the nervous system to modify itself, either functionally or structurally [6], could potentially compensate for inaccuracies in the emulated model. Our study investigates the extent to which these properties can assist in restoring already lost or distorted information and maintain functional accuracy in brain emulation.
Another side-focus is the spatial contribution of different brain regions to the overall impact of measurement errors. The brain operates as an intricate network of differently inter-connected regions, each one playing a distinct role in perception, memory and other cognitive functions. Therefore, errors in imaging specific areas may have different impacts on the overall model, depending on the importance of the regions' role. Moreover, there could also be a linkage between their connectivity and the extent of their contribution to error propagation. Our study explores how errors coming from different regions affect the emulation reliability.
By answering to these questions, we aim to develop a framework for quantifying the impact of measurement errors on brain emulation. This, could help establishing thresholds and levels, where errors become critical and concurrently, provide a methodology of accuracy-improvements even after acquiring imperfect data.

## 1.4 Thesis Structure

This dissertation is organized into 7 chapters, each focusing on a key aspect of the research process, from the theoretical background to experimental methods, the results and, finally, the interpretation and significance of findings.

Starting from the broader context of the research, the introduction aims to discuss the relevance of studying neural connectivity and dynamical models in neuroscience. The study's key objectives and hypotheses are presented, along with an overview of the main challenges that we aim to address.
We then review the relevant literature on brain network modelling, tracing its development from early, basic models to the more sophisticated approaches used today. Additionally, we discuss the models that are favored for long-term modelling and highlight previous studies that emphasize the importance of further investigating measurement errors in brain modelling.
Next, the methodology chapter outlines the design and implementation of the selected models used for the neural simulation. It describes the process of building the connectivity adjacency matrices, introduces the models, and explains how noise and learning are incorporated into the simulations. Finally, the methods used for hyperparameter tuning and evaluating model performance are also covered.
The Results chapter presents the outcome of the simulation experiments, exploring the effect of different, scaled, noise levels, learning rates, and timepoint variations on neural dynamics. Both qualitative and quantitative analyses are provided, including error evaluations, visualizations and curve-fitting statistical results.
In the following Discussion chapter, the findings are interpreted in the theorectical context of brain network modelling and neuroscience. Limitations of the models are critically assessed, and potential improvements and future directions are suggested.
The final chapter summarizes the major contributions of the thesis, revisiting the research objectives and how they were met. The implications of the findings for future work in neural network simulations and computational neuroscience are discussed, and final thoughts on the overall impact of the research are provided.
The appendices contain references to the literature cited throughout this dissertation. These citations serve to support the claims made in each chapter and provide context for further exploration of the relevant studies that inform this research.

# Chapter 2

# Literature Review

## 2.1 Overview of Brain Modelling

Chapter 2. *Overview of brain modelling* **Brain modelling** is an interdisciplinary field that combines neuroscience, computational science and engineering aiming to create comprehensive simulations of the brain's structure and function [7]. Towards the ultimate goal of understanding the processes, predicting the behavior and potentially emulating digitally the brain, computational and mathematical modelling of neural populations has been a focal point of computational neuroscience research.
The field has evolved significantly in recent decades, driven by advances in biology, computer science and technology. The groundwork for more sophisticated models aiming to capture complexity of brain functions came from the pioneering work of *McCulloch and Pitts (1943)*, who developed a logical calculus of the ideas immanent in nervous activity [8]. Moreover, a significant milestone of the domain was the development of the *Hodgkin-Huxley model (1952)*, which provided a more detailed, mathematical description of the electrical properties that excitable cells such as neurons, present [9]. This model was pivotal in unraveling how neurons communicate through electrical impulses, and laid the foundation for subsequent single-neuron-level models.

In recent-years, progresses in computing power have led to the prominence of large-scale brain models that aim to simulate entire brain regions, or even the whole brain. One of the most ambitious projects is the *Blue Brain Project*, initiated by *Markram et al. (2006)*, which focuses on creating a digital reconstruction of the rodent brain at a cellular level [10]. BBP simulates neural

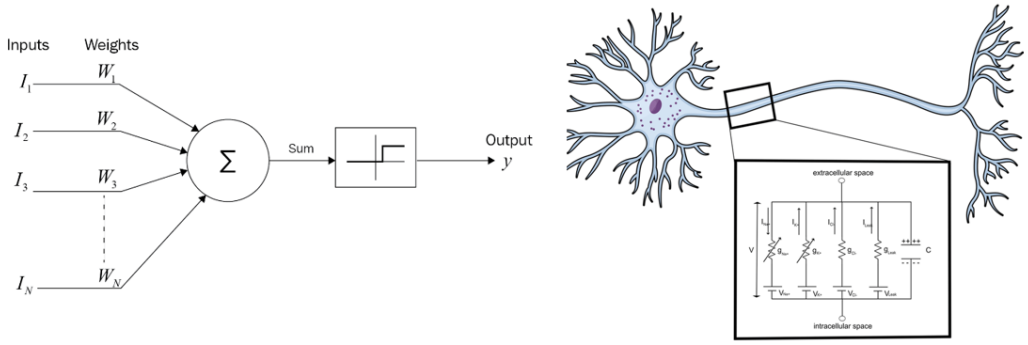


FIGURE 2.1: (a) McCulloch-Pitts neuron model, representing a simplified artificial neuron functioning as a binary threshold unit. (b) Biological neuron, illustrating complex structures like dendrites, axon, and synapses involved in signal transmission.

microcircuits via numerous supercomputers, thus, providing insights into brain function and pathology.
Another significant contribution is, undoubtedly, the *Human Brain Project*, a large-scale European research initiative, aimed at building a comprehensive model of the human brain [11]. For this goal, data from a plethora of projects get integrated to create a unified model, robust enough for both research and clinical applications. The Human Brain Project emphasizes the importance of collaboration across disciplines and the use of high-performance computing to manage and analyze large datasets.
Despite the aforementioned scientific and technological advancements, brain modelling faces several challenges. One of the primary obstacles is the accurate representation of the brain's vast complexity. Containing over 86 billion neurons, each holding its individuality with cellular traits such as excitability, while simultaneously being connected by synapses creating super-complex networks, the brain is very challenging to model because capturing this level of detail in a digital form, requires immense computational power and sophisticated algorithms.
In addition, measurement errors during data acquisition introduce variability and noise, complicating the process of creating accurate models. Techniques such as the Magnetic Resonance Imaging (MRI) and Diffusion Tensor Imaging (DTI) are

commonly used to capture the structure, but come with limitations in terms of noise and resolution constraints. *Galasser et al. (2016)* in the *Human Connectome Project* highlights these challenges and underscores the need for improved imaging techniques and data processing methods[12].
The future of brain modelling lies in the integration of multi-scale data from bio-molecular to behavioral levels, and the continuous improvement of imaging and computational techniques. Advancements in AI and Machine Learning may hold promise for the enhancement of models' accuracy and efficiency. Collaborative efforts, open data initiatives and interdisciplinary efforts will be vital for overcoming current limitations assisting in the development of this dynamic, rapidly evolving field, ultimately contributing to the goal of WBE.

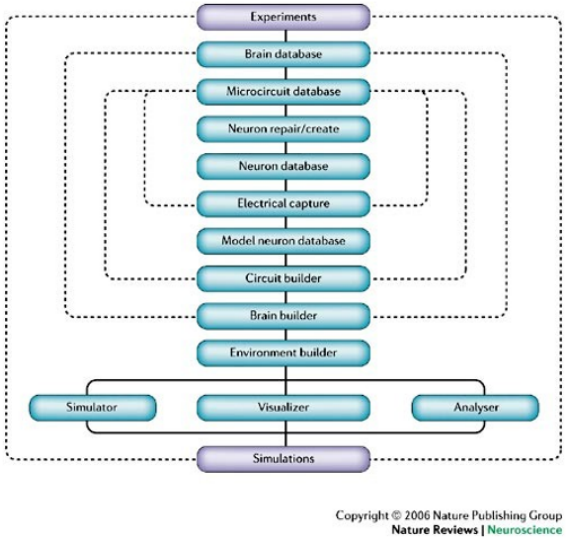




FIGURE 2.2: a) NEURON software flowchart, illustrating the computational modelling process used for simulating neurons and networks. (b) Blue Brain Project logo, representing a pioneering initiative to digitally reconstruct and simulate the brain at a cellular level. (c) Human Brain Project logo, symbolizing the broader effort to advance brain research through large-scale simulation and data-driven neuroscience.

## 2.2 Types of brain models used in long-term activity studies

Long-term brain activity studies focus on elucidating the way brain functions, processes and structures evolve over extended periods, ranging from minutes to hours or even longer. These studies play a crucial role in diving further into chronic neurological conditions, cognitive aging, learning processes and the long-term effects of therapeutic interventions. A plethora of models can be used for such cause, and can be categorized based on their scale, purpose, and the methodologies employed. [13]

- **Neural Mass Models:** Models that simplify larger populations of neurons into average activity patterns. These models are useful for studying large-scale brain dynamics and long-term oscillatory behavior

- **Network Models:** Models that simulate the interactions between different brain regions or within specific neural circuits. May vary in complexity, from simple network representations to highly detailed simulations involving thousands of interconnected neurons.

- **Biophysical Models:** Models that aim to represent the thorough properties of neurons and synapses. The aforementioned *Hodgkin-Huxley model (1952)* is a foundational biophysical model that describes the ionic mechanisms underlying action potentials in neurons. These models are essential for studies that require precise simulations of neuronal behavior and plasticity mechanisms.

- **Large-Scale Brain Simulations:** These models integrate data from multiple levels of organization, including molecular, cellular, and network scales. Both the *Blue Brain Project* and the *Human Brain Project* aim to create such comprehensive models of entire brain regions or the whole brain.

These simulations are particularly valuable for exploring long-term changes in brain function and structure, such as those resulting form chronic conditions or lifelong learning.

Long-term brain activity research provides valuable information about the stability and plasticity of brain networks and, therefore, help to uncover the mechanisms underlying chronic conditions and long term cognitive processes. By leveraging numerous types of brain models, researchers study the intricate dynamics of the brain activity and ultimately contribute to advancements in neuroscience and targeted interventions for neurological disorders.

## 2.3 Previous studies on measurement errors in brain activity

Measurement errors in brain activity studies are a significant concern as they can lead to inaccurate models and misinterpretations of neural processes. These errors can arise from various sources including limitations in imaging technologies, inconsistencies in data acquisition, and noise introduced during measurement process. In this section previous studies that have investigated the impact of measurement errors on brain activity, data and modelling are being reviewed.

- **Impact of Measurement errors in fMRI:** *Functional Magnetic Resonance Imaging (fMRI)* is one of the most extensively used techniques of measuring brain function, and is performed by recording changes in blood flow. However, it is susceptible to many noises sources such as physiological (e.g. heartbeat and respiration), thermal noise and scanner-related artifacts. There have been many studies demonstrating that these noise sources can significantly affect the reliability and reproducibility of fMRI results. For example, *Friedman and Glover (2006)* highlighted the influence of

physiological noise on fMRI signal variability and the importance of correction methods to improve data accuracy. Their work underscores the need for advanced preprocessing techniques to mitigate the impact of measurement errors on fMRI studies [14].

- **EEG & MEG Measurement Errors:** *Electroencephalography (EEG)* and *Magnetoencephalography (MEG)* are techniques that measure the electrical and magnetic activity of the brain, respectively. These methods are susceptible to noise arising from inconsistent electrode placement, signal artifacts, and environmental interference. Research has shown that noise can significantly impact the quality of EEG recordings. For instance, a study exploring various noise sources indicates that signal quality can be improved through careful data cleaning and denoising techniques *(Sharma & Singh, 2022; Wu et al., 2021)*. These findings underscore the importance of implementing robust preprocessing methods to enhance the accuracy of EEG measurements, ultimately contributing to more reliable brain function assessments [15] [16].

- **Diffusion Tensor Imaging (DTI) and Measurement Variability:** *Diffusion Tensor Imaging DTI* is an MRI form that maps the diffusion of water molecules in brain tissue, revealing the structure of white matter. Noise in DTI can be caused either by motion artifacts, inaccuracies in tensor estimation or often by factors like low signal-to-noise ratio (SNR). *Jones and Cercignani (2010)* reviewed the sources of variability in DTI measurements and discussed methods to improve the robustness of diffusion metrics. Their work highlights the challenges of obtaining reliable DTI data and the importance of addressing measurement errors for accurate white matter analysis [17].

- **Quantitative Assessments of Measurement Error Impact:** There are several studies that have quantitatively evaluated the effect of measurement errors on brain activity data. For example, *Gorgolewski et al. (2013)* completed a large-scale

review of fMRI data from several studies to assess the **reproducibility** of brain activity patterns. They discovered that measurement noise and preprocessing decisions had a substantial impact on the consistency of results, highlighting the need of uniform data collection and analysis processes [18].

In summary, measurement errors show significant challenges in brain activity studies, affect the accuracy and reliability of the data and subsequent models. Previous research has identified various sources of these errors and proposed methods to mitigate their impact.

# Chapter 3

# Methodology

Chapter 3. *Methodology*

## 3.1 Description of the selected brain models

### 3.1.1 Kuramoto model

Oscillators are systems that exhibit periodic behavior. The rhythmical activity of each component can be described as a physical variable that evolves regularly in time and when reaching a specific threshold, emits a pulse (action potential in the case of neurons) that propagates through the oscillator's respective neighborhood. The effect of an emitted pulse alters the current state of neighbors by modifying their periods. This disturbance depends on the state of each oscillator receiving the external pulse, and can be studied in terms of a phase-shift
The Kuramoto model is a mathematical framework used to describe synchronization phenomena in a system of coupled oscillators [19]. The system consists of $N$ coupled phase oscillators $\theta_i(t)$ having natural frequencies $\omega_i$, distributed with a given probability density $g(\omega)$, and whose dynamics are governed by:

$$\theta_i = \omega_i + \sum_{j=1}^{N} K_{ij} \sin(\theta_j - \theta_i), \quad i = 1, ..., N \quad and \quad 0 \leq \theta_i \leq 2\pi$$

- Natural frequency $\omega_i$ : The rate at which oscillator i would rotate if it was isolated.

- Coupling term: The sine of the phase difference between oscillators $i$ and $j$ modulated by the coupling strength $K$, captures how the phase of one oscillator affects the phase

of others.

Therefore, although each oscillator runs independently, with its own frequency, the coupling tends to synchronize it to the rest. In the case of sufficiently weak coupling, the oscillators run incoherently, whereas beyond a certain threshold point, collective synchronization emerges spontaneously. For a system of $N$ oscillators, the natural frequency $\omega_i$, representing the rate at which oscillator moves through its cycle without external influence, is drawn from a distribution, reflecting the heterogeneity in the system.
The degree of synchronization within the system is quantified using an order parameter $r$ , defined as:

$$re^{i\psi} = \frac{1}{N}\sum_{j=1}^{N} e^{i\theta j}, \quad 0 \leq r \leq 1$$

Where $r$ ranges from 0 (complete desynchronization) to 1 (complete synchronization). The coupling strength $K$ is a control parameter that dictates the strength of the oscillators' interaction. When $K = 0$, the oscillators run independently at their natural frequencies. As $K$ increases, the influence of coupling term grows, driving the oscillators toward synchronized behavior. The transition from incoherence to synchronization is a type of bifurcation where, beyond a critical coupling strength $K_c$, the oscillators begin to synchronize.

The Kuramoto model has a plethora of applications, including biological systems, like neuronal networks, where synchronization can elucidate rhythmic activities. However, while it provides significant insights into the mechanisms of synchronization, it is essential to recognize its limitations, especially in simplifying more complex interactions [20].

### 3.1.2 Izhikevich Model

The Izhikevich model, introduced by *E.M. Izhikevich (2004)*, is a mathematical framework used to describe the dynamics of spiking and bursting in neurons. It was firstly brought as an alternative to the prior Hodgkin-Huxley model, which despite its biological realism appears to be sufficiently more computationally intensive. The Izhikevich model balances these aforementioned aspects, thereby making it one of the most renowned neural-dynamics models, as even its small number of parameters, can realize a variety of neural-firing patterns. The equation is described as follows:

$$\dot{v} = 0.04v^2 + 5v + 140 - u + I = f_0,$$
$$\dot{u} = a(bv - u) = g_0$$

Furthermore, Spiking conditions are written as follows:

$$If \quad v \geq 30\,[mV], \quad then : u \leftarrow \{\, c\,, u + d \text{otherwise.}$$

Where, the state variables $v$ and u correspond to the membrane potential of the neuron and membrane recovery variable, respectively. The parameters are $a$, $b$, $c$, $d$ and $I$. Here, $a$, $b$ and $I$ represent the time-scale of the recovery variable u, the sensitivity of the recovery variable u to $v$ and the synaptic current respectively, while $c$ and $d$ are reset values. After the spike reaches its apex, the state variables $v$ and $u$ are reset according to the equation above.
In theory, the first equation part was obtained by fitting the spike initiation dynamics of a cortical neuron, so that the membrane potential $v$ has mV scale and the time has ms scale. The resting potential in the model is between -70 and 60 mV depending on the value of b [21]. More specifically:

- The parameter a describes the timescale of the recovery variable u. **Smaller values** result in **slower recovery**. A typical value is a=0.02.

- The parameter b describes the sensitivity of the recovery variable u to the subthreshold fluctuations of the membrane

potential $v$. **Greater values** couple $v$ and u more strongly resulting in possible subthreshold oscillations and **low-threshold spiking** dynamics. A typical value is $b = 0.2$. The case $b < a(b > a)$ corresponds to saddle node (Andronov-Hopf) bifurcation of the resting state.

- The parameter c describes the after-spike value of the membrane potential $v$ caused by the fast high-threshold $K^+$ conductance. A typical value is c = -65 mV.

- The parameter d describes after-spike reset of the recovery variable u caused by slow high-threshold $Na^+$ and $K^+$ conductance. A typical value is d=2.

#### Hebbian Learning

**Hebbian Learning** is a foundational concept in neuroscience that explores how neurons can adapt and change based on experience. The theory was first introduced by Canadian psychologist *Donald Hebb in 1949*and is often summed up by the phrase **"cells that fire together, wire together"**. This idea indicates the notion that when two neurons repeatedly activated at the same time, the connection between them becomes stronger. Over time, this process enhances the efficiency of communication between neurons, leading to changes in behavior, learning, or memory.
The core principle of Hebbian learning lies in synaptic plasticity. When one neuron (the presynaptic neuron) consistently triggers the activation of another (the postsynaptic neuron), the synaptic connection between the two is strengthened. This change at the synapse is a biological mechanism that underpins learning and memory formation in the brain. This idea was a significant leap in understanding how the brain works, marking a shift from earlier theories that thought of the brain as a static organ. Hebb's theory highlighted that the brain is highly dynamic, with neural circuits continually adjusting based on experience.

Hebbian learning has also had a significant influence on the development of artificial intelligence. Early models of artificial neural networks (ANNs) borrowed heavily from Hebbian principles . Although these early models were relatively simple, they laid the groundwork for more sophisticated learning algorithms used in today's AI systems.
In summary, Hebbian learning is a vital principle that has influenced both neuroscience and artificial intelligence. It explains how repeated experience can shape the brain, strengthening the connections between neurons and facilitating learning and memory. [6]

## 3.2 Data Collection Methods

We utilized imaging data from the Human Connectome Project (HCP), from *Van Essen et al. 2012* [22], specifically the S1200 release, which includes structural, diffusion, and resting-state functional MRI data. HCP comprised brain activity from 280 patients and all data were acquired using a *Siemens Skyra 3T MRI scanner* equipped with a customized *SC72 gradient insert*.
For the structural data, *T1-weighted 3D MPRAGE scans* were collected with a repetition time (TR) of 2400 milliseconds and echo time (TE) of 2.14 milliseconds. The inversion time (TI) was set to 1000 milliseconds, with a flip angle of 8 degrees and a field of view (FOV) of 224x224 millimeters. These scans provided high-resolution images with 0.7 millimeter isotropic voxels. Additional parameters included a bandwidth of 210 Hz/pixel, *iPAT of 2*, and a total acquisition time of 7 minutes and 40 seconds.
Diffusion-weighted imaging (DWI) was performed using *spin-echo EPI* sequences with multiple b-values (0, 1000, 2000, and 3000 $s/mm^2$) in approximately 90 gradient directions. The scans were acquired with a TR of 5520 milliseconds and a TE of 89.5 milliseconds, with a flip angle of 78 degrees and a matrix size of 168x144. The voxel size was 1.25 millimeters isotropic, and 111 slices were obtained for each scan. A multiband factor of 3 was used to reduce acquisition time, and echo spacing was set at 0.78 milliseconds.

Resting-state functional MRI (fMRI) data were collected using a *gradient-echo EPI* sequence, with a TR of 720 milliseconds and a TE of 33.1 milliseconds. The field of view for these scans was 208x180 millimeters, and images were captured with 2.0 millimeter isotropic voxels across 72 slices. Resting-state sessions consisted of 1200 frames over a duration of 14 minutes and 33 seconds. Participants were instructed to keep their eyes open and fixate on a projected cross-hair. The resting-state fMRI data were denoised using *ICA-FIX (Independent Component Analysis with FSL FIX)*, ensuring spurious correlations were removed (Smith et al., 2013) [23].

The structural and diffusion imaging data were preprocessed as part of the HCP pipeline. For the T1-weighted MRI scans, preprocessed images were downloaded directly from the HCP dataset. Diffusion imaging data underwent additional preprocessing, including a bias field correction using FSL's fast tool. A *nodif brain mask*, provided as part of the diffusion imaging data, was applied to the mean b0 image for each subject. Freesurfer's parcellated brain regions (based on the Desikan atlas) were then registered to the b0 image using the boundary-based registration tool bbregister.

These registered regions (82 in total, 34 cortical and 7 subcortical regions per hemisphere) were used as input for deterministic fiber tracking in *DSI-Studio Yeh, Wedeen, & Tseng, 2010*. To reconstruct the diffusion images, generalized *q-sampling imaging (GQI)* was employed with a diffusion sampling length ratio of 1.25 *(Gangolli et al., 2017)* [24]. Fiber tracking was initialized with sub-voxel seeding, generating 1 million streamlines per subject. Streamlines with lengths shorter than 10 millimeters or longer than 300 millimeters were discarded to ensure realistic connections. Additionally, topology-informed pruning was applied to further refine the connectivity results *(Yeh et al., 2019)* . The final output was a symmetric connectivity matrix for each subject, detailing the number of streamlines connecting each pair of brain regions.

For resting-state fMRI data, preprocessed BOLD signal data were obtained from the HCP's FIX-denoised release, which consisted of 1200 time points of BOLD activity for each subject. Freesurfer's

parcellated regions were registered to MNI space using FSL's *fnirt* tool. For each brain region, the BOLD signal was extracted using FSL's fslmeants tool, and time-series data were obtained for all cortical and subcortical regions. A bandpass filter was applied to each region's BOLD signal to retain frequencies between 0.01 Hz and 0.2 Hz, which is typical for functional connectivity analyses. Functional connectivity (FC) matrices were then generated by calculating Pearson correlation coefficients between time-series from different brain regions.

## 3.3 Data Visualization

A generalization of the analysis was implemented, with matrices from all patients (n=280) being averaged, ensuring the capture of the general connectivity patterns across the population, rather than individual variations.
Since raw connectivity values can sometimes include outliers, we also applied a winsorization process to the averaged matrix, to limit the impact of such extreme values. Specifically, values below the 10th percentile and above the 90th percentile were capped. The matrix was then normalized to a [0, 1] range for consistency in further computations and better visualization.
To better understand the underlying network structure and the connectivity between the 82 regions of interest (ROIs), the adjacency matrix was visualized using two primary methods: heatmaps and 3D brain network plots.
Heatmaps were used in order to provide a clear and immediate visual representation of the connectivity strength between brain regions. The adjacency matrix, which represents the number of streamlines connecting each pair of regions, was displayed as a color-coded grid. Each entry in the matrix corresponds to the connection strength between two ROIs with color intensity indicating the number of connections (or number of streamlines). This visualization helped to identify key connectivity patterns, such as strongly or sparsely connected areas, and provided an overview of the global structure of brain networks before the noise introduction. [25]

Moreover, to provide a more intuitive, realistic, and spatially-aware visualization of the brain's connectivity network, *BrainNet Viewer (Xia, Wang & He, 2013)* [26] was employed. This tool allowed the representation of the adjacency matrix in a 3D brain model, with nodes representing the ROIs and edges representing the connections between them. The strength of connections was represented by the thickness or colors of the edges in the 3D plot, offering insights into which regions of the brain were most influential on the overall network.

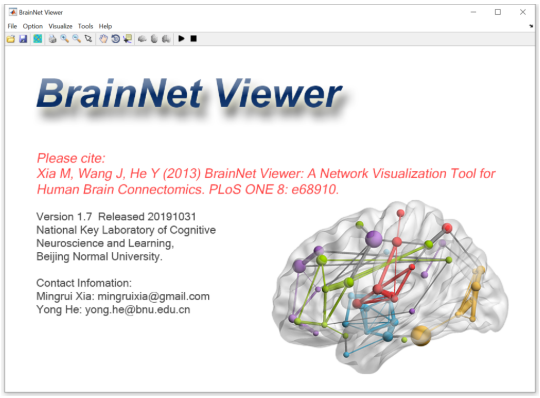


FIGURE 3.1: BrainNet Viewer: A Tool for Visualizing Brain Network Data

### 3.3.1 Introduction of noise

To achieve the goal of assessing the robustness and accuracy of brain models in the presence of measurement errors, noise was introduced into the original adjacency matrix. The adjacency matrix represents the "perfect" connectivity between different ROIs in the brain, and noise was added to simulate real-world imperfections in data collection, such as sensor inaccuracies, environmental interference, or signal processing errors.
The original connectivity matrix was generated by the averaging the connection weights across multiple participants from the Human Connectome Project. This matrix served as the baseline for comparison, representing the "control" or error-free brain network. Noise was introduced into the matrix using a controlled approach, where a random Gaussian noise matrix was generated and added to the original matrix. The amount of

noise added was controlled by a **noise factor g** which scaled the noise magnitude. A specific generating seed was also implemented to ensure the reproducibility of the results.
Mathematically, the noisy connectivity matrix $_noisy$ was generated as:

$$W_{noisy} = W_{original} + gxN$$

Where $W_{original}$ is the control adjacency matrix, g is the noise factor, and N is a matrix of random values sampled from a Gaussian distribution with mean zero and unit variance. To evaluate the effect of increasing measurement errors, noise was introduced at different levels, ranging from 0.1 to 1.0 in steps of 0.1. This allowed for a systematic exploration of how varying degrees of noise affect the connectivity matrix and, subsequently, the brain models used in the study. At each level of noise, a new matrix was generated, resulting in a series of matrices with progressively higher levels of error. The impact of noise was first visualized using boxplots, showing how the distribution of connection weights changed as the noise factor increased. This helped in identifying the general trends in connectivity variations as errors were introduced. Additionally, the mean absolute difference between the control (error-free) connectivity matrix and the noisy matrices was calculated and plotted. This allowed for a quantitative assessment of the magnitude of change in connectivity due to noise, providing insights into the extent of disruption caused by increasing noise levels.

### 3.3.2 Model Simulations

We employed two widely recognized models for simulating brain activity, aiming to assess their robustness in the presence of measurement errors. These models were:

- **Kuramoto Model:** Each brain region was treated as a single neuron, an oscillator, with its phase evolving over time. Each ROI was assigned random initial conditions, phases $\theta \in [-\pi, \pi]$ drawn from uniform distributions ensuring an even spread of phases at the start of the simulation. Random natural frequencies $\omega \sim \mathcal{N}(0, 1)$ were sampled from

a normal distribution with mean $\mu = 0$ and $\sigma = 1$, which ensured that the oscillators had different intrinsic dynamics, simulating variability in neural activity between brain regions. Coupling strength $K$ was set to 0.5.

- **Izhikevich Model:** Each brain region was treated as a single neuron, and its activity evolved according to predefined neuronal firing rules. The external input current $I_{ext}$ is a combination of a baseline current of 3 units, an oscillatory input with a frequency of 2 Hz, contributing to the modulation of neuronal activity, and noise added to each neuron's input current, simulating random fluctuations that impact the neural dynamics. In addition, the synaptic input $I_{syn}$ represents the influence of other neurons in the network that are spiking. At each timepoint, neurons that have spiked at the previous timestep contribute to the current synaptic input. This means that for each neuron, the synaptic input is calculated by summing the contributions from other neurons that spiked previously, weighted by their respective connection strengths in the weight matrix $W$. If it's the first time step (i.e., $t = 1$), no neurons have spiked yet, so the synaptic input is set to zero.

The simulations were divided into three phases. First, the system ran up to the branching point $k$ without noise, allowing it to evolve naturally. Once it reached k, which represents the second phase, noise was introduced to the system based on different error factors, and each simulation was continued to the third phase, until the end of the simulation time.
For our main simulation type, we used a total simulation time of **30 seconds** (30,000 ms), and an individual time-step of 1ms. At an initial timestep k=5000 ms, noise was introduced into the connectivity matrix in the aforementioned way, allowing for an analysis of the models' pre- and post- noise behaviors.
Hebbian learning was implemented based on the weight updating rule, which reflects that the coupling between two neurons increases when their phases or activities are more closely

aligned respectively. A learning rate n controlled the size of new weights-adjustment indicating the pace of the system's plasticity.
Both learning rate, which controlled the effect of Hebbian Learning and k, the time-point when noise got introduced to the system, were later explored for all models to assess the adaptability of the system in the presence of noise.

### 3.3.3 Analysis of Errors over Time

For each noise level, the difference between the noisy and noise-free simulations was calculated over time. The sum of absolute differences across all regions (ROIs) at each time point provided a measure of how the noise altered the model's behavior regardless the respective ROI. The plot of total errors across timepoints, for each noise level (from 0.1 to 1.0), showed how the simulations diverged from the control conditions as time progressed and with increasing noise. This gave insight into the cumulative impact of noise on the synchronization or firing rates of the brain regions.

### 3.3.4 Noise-introduction timepoint, Hyperparameter tuning

Different values of k were tested, ranging from 1 ms to 30,000 ms. To ensure consistency and fairness in comparing the effects of noise introduced across various k timepoint scenarios, the post branching point simulation continued for a fixed additional time period of 10,000 ms in all instances. This fixed post-noise simulation time is crucial because, without it, larger k values would inherently lead to smaller errors, creating invalid impressions.
Furthermore, the error measurement was carefully handled by focusing only on the time period after the noise got introduced. For each k, the error was computed by taking the mean of the sum of absolute differences between the noisy system and the original system (without noise) from time k onwards. This ensures that the error reflects only the system's behavior after noise

is applied, preventing any bias in the results due to longer pre-noise periods. By maintaining a consistent post-noise time for all k values and calculating the error in this focused period, the simulation ensures a fair and meaningful comparison of how noise affects the system at different points in time.
In addition to the computational modelling of the Kuramoto system, we employed statistical methods to assess the significance of the observed fluctuations in mean error across different k-timepoints. Specifically, we conducted linear regression analyses to evaluate the relationship between k and the corresponding mean error.
The regression model was formulated as follows:

$$MeanError = \beta_0 + \beta_1 \cdot k + \epsilon$$

Where $\beta_0$ represents the intercept, $\beta_1$ denotes the slope, and $\epsilon$ is the error term.

After fitting the model, we examined the p-value associated with the slope to determine whether there was a statistically significant relationship between k and mean error. A p-value less than the threshold of 0.05 would indicate a significant relationship, allowing us to reject the null hypothesis that there is no effect of noise introduction timing on the error progression, within 95% level of significance.

### 3.3.5 Learning-Rate, Hyperparameter tuning

To explore the best adaptation strategy in the presence of noise, the learning rate of the models was varied logarithmically across a range of values (from 0.1 to 1). By calculating the mean of the differences between the noisy and control conditions across different learning rates, the optimal learning rate for minimizing error was identified.

### 3.3.6 Spatial contribution to final Error

The error contribution of each brain region (ROI) to the total error was analyzed across different noise levels. For each noise level, the sum of absolute differences for each ROI was calculated, providing a measure of how each region contributed to the error. Moreover, to understand the relative importance of each ROI, the error contributions were normalized and averaged across all noise levels. Spearman's coefficient was calculated between both models' error-contribution rates and their relative connection strengths. This allowed for identifying which regions were most sensitive to noise and contributed most to the overall error. The final plot of ROI-wise error contributions showed the spatial distribution of the noise effects and highlighted the regions' most vulnerable to measurement errors.

# Chapter 4

# Results

Chapter 4. *Results*

## 4.1 Presentation of findings

### 4.1.1 Data Visualization

The starting point for the simulations is the structural connectivity matrix representing the average functional connectivity between N= 82 Regions of Interest (ROIs) in the brain. This adjacency matrix is constructed from the HCP dataset by averaging the connectivity weight across all subjects, yielding a matrix that forms the basis for simulating the neural dynamics.
The adjacency matrix, is a symmetric matrix where each element, W(i,j) represents the connection strength between two ROIs, i and j. This matrix is winsorized and normalized to cap extreme values and rescaled between 0 and 1, ensuring numerical stability and interpretability. Rows and columns are ordered according to anatomical criteria, such that all left hemisphere regions are listed first, followed by all right hemisphere regions.

Within each hemisphere, the ordering of the regions is the same, so that the first-listed left hemisphere region and first listed right hemisphere region correspond to homologous areas. With this ordering, we see two clear blocks of increased connectivity: one in the upper-left quadrant and one in the lower-right quadrant. These two blocks represent the intrahemispheric connectivity of the left (upper left quadrant) and right (lower right quadrant) hemispheres. Interhemispheric connectivity is depicted

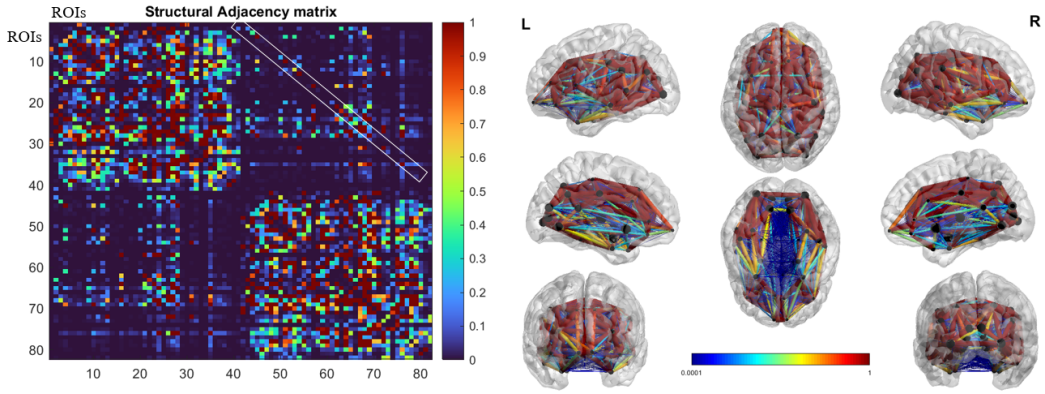


FIGURE 4.1: Left: Adjacency matrix illustrating the connections between brain regions. Right: 3D visualization of the brain's connectivity structure generated using BrainNet Viewer.

in the upper right and lower left quadrants. The box in Figure 4.1 highlight subdiagonal elements of the matrix that encode connectivity between homologous regions in the left and right hemispheres. From this anatomically informed matrix-representation, we see that intrahemispheric connectivity is stronger than interhemispheric connectivity, and that there is a tendency for homologous regions in opposite hemispheres to be connected with each other.
Finally, by projecting the adjacency matrix into the brain's anatomical space, the connectivity patterns seen and explained earlier in the matrix become visually aligned with the brain's physical regions. This approach validates the observed connectivity by showing that the abstract graph-based patterns correspond to plausible real-world anatomical relationships. In this way, the anatomical projection graph reaffirms the meaningfulness of the connectivity patterns in a biologically realistic context.

### 4.1.2 Noise Introduction & Weight Divergence

To investigate the robustness of the network's structural connectivity to noise, we introduced varying levels of noise into the control adjacency matrix and compared the resulting weights to the original ones. Noise levels were incrementally increased,

based on error-factors varying from 0.1 to 1, simulating progressively larger disturbances in the connectivity data.

Figure 4.2 (a) presents a boxplot showing the distribution of weights for each noise factor. As the noise factor increases, the spread of the weight distribution becomes wider, indicating an increased divergence in the connectivity patterns. This widening of the distribution reflects how higher noise levels introduce more variability and uncertainty into the network's connectivity.

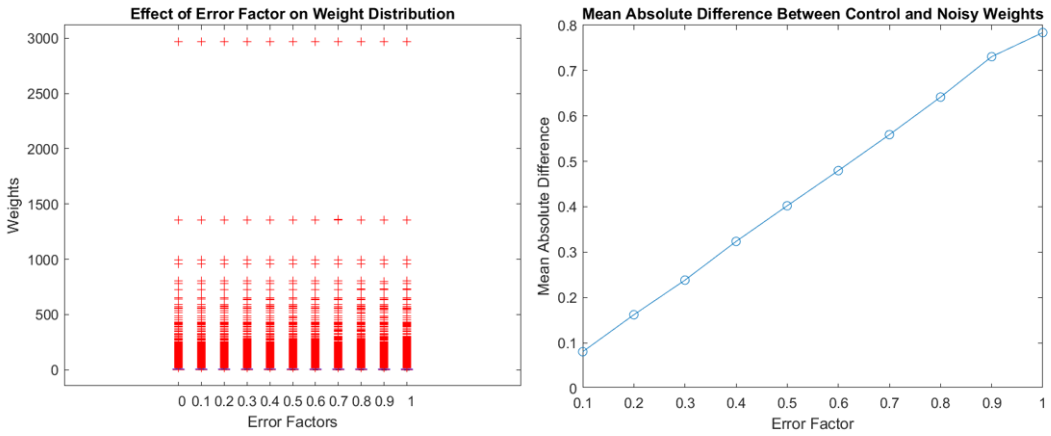


FIGURE 4.2: (a) Boxplot showing the distribution of weights for each noise factor. (b) Mean absolute difference between the control weights and the noisy weights across different error factors.

In addition, Figure 4.2 (b) plots the mean absolute difference between the control weights and the noisy weights across different error factors. The plot shows a clear upward trend, demonstrating that as the noise factor increases, the average difference between the noisy and control weights grows steadily. This illustrates that higher noise levels cause a significant deviation from the original structural connectivity, affecting the network's overall coherence.

### 4.1.3 Kuramoto model

The Kuramoto model was used to simulate the impact of noise on the synchronization dynamics of the network. In this model, various error factors were introduced to observe their effect on the network's behavior over time.
Figure 4.3 demonstrated that, in the case with no Hebbian Learning, as simulation time progresses, the mean error between noisy and control conditions steadily increases. This suggests that the cumulative impact of noise leads to a growing divergence in the network's dynamic behavior compared to the control case.

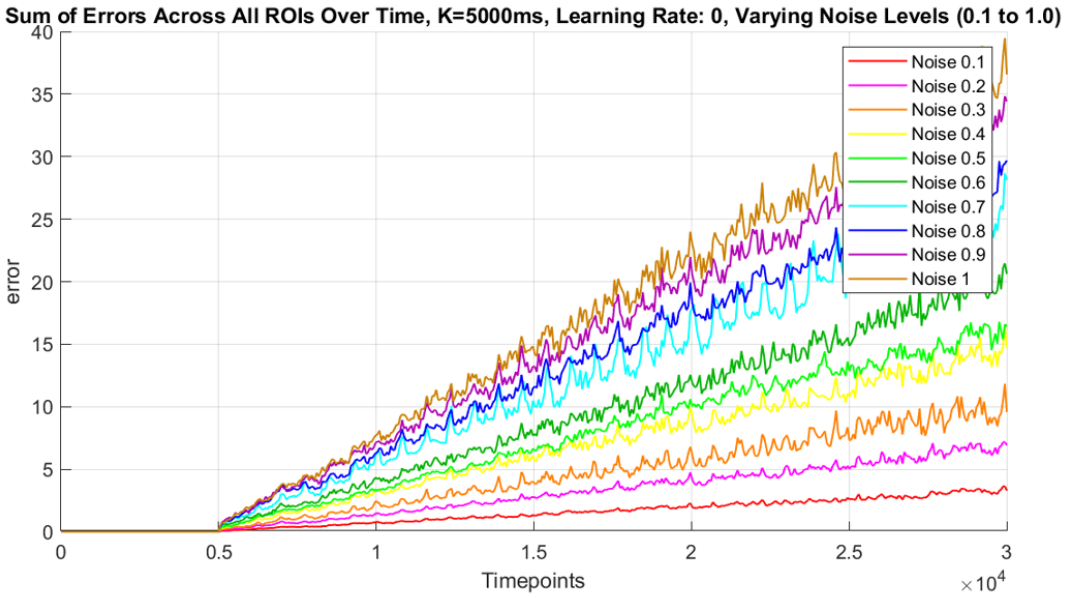


FIGURE 4.3: The Kuramoto model simulation of network synchronization dynamics under noise influence without Hebbian learning. The figure shows that as the simulation progresses ($k$ = 5000 ms and learning rate = 0)

Furthermore, a clear correlation can be observed between the magnitude of the error factor and the resulting noise. The larger the error factor introduced into the system, the more significant the divergence from the control scenario. These results highlight the sensitivity of the network's synchronization dynamics to noise and suggest that even small perturbations can lead to considerable disruptions over time, especially when accumulated.

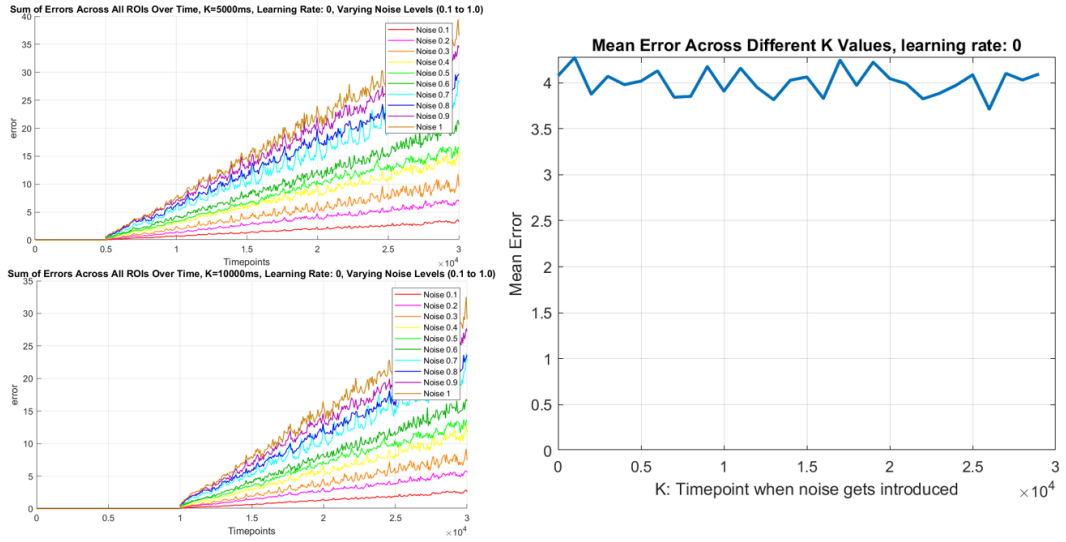


FIGURE 4.4: Kuramoto model: The impact of noise introduction timepoint $k$ on network dynamics. (a) The error progression over time for two different instances of $k$, $k = 5000ms$ and $k = 10000ms$ with $learningrate = 0$ (b) The mean error as a function of the $k$ hyperparameter.

In addition to analyzing the effect of different noise levels, the timepoint $k$ – when noise was introduced into the system – was also varied to investigate its impact on the network's dynamics. The results showed that while some minor fluctuations were observed when adjusting the timepoint $k$, the overall trend remained largely unaffected. Figure 4.4 illustrates that for multiple values of $k$, the error progression over time follows a relatively consistent trajectory, with only minimal disturbances along the curve. This suggests that the exact moment when noise is introduced into the system has limited influence on the network's long-term behavior. Statistical analysis through linear regression revealed a significant p-value of 0.012207 for the slope, indicating that the fluctuations in error are statistically significant at a 95% level of significance. However, despite this significance, there is no discernible trend of increase or decrease in the mean error as a function of $k$. Therefore, while the timing of noise introduction affects the mean error, the relationship appears complex and does not point to a straightforward pattern. In the case of Hebbian learning, Figure 4.5 which is depicting the relationship between mean error and timepoints illustrates that, as time progresses, a more intricate and complex relationship

emerges between error factors and errors. Unlike the scenario without learning, where the errors displayed a more consistent trajectory, the introduction of a learning rate introduces notable fluctuations in the error progression over time. Specifically, the errors do not exhibit a steady slope, indicating that they are significantly more variable when learning is incorporated into the system.
Additionally, the analysis of mean error as a function of different learning rates suggests that higher learning rates may lead to smaller mean errors; however, this reduction in error comes at the cost of increased fluctuations. To evaluate the significance of this observation quantitatively, further statistical testing should be conducted.

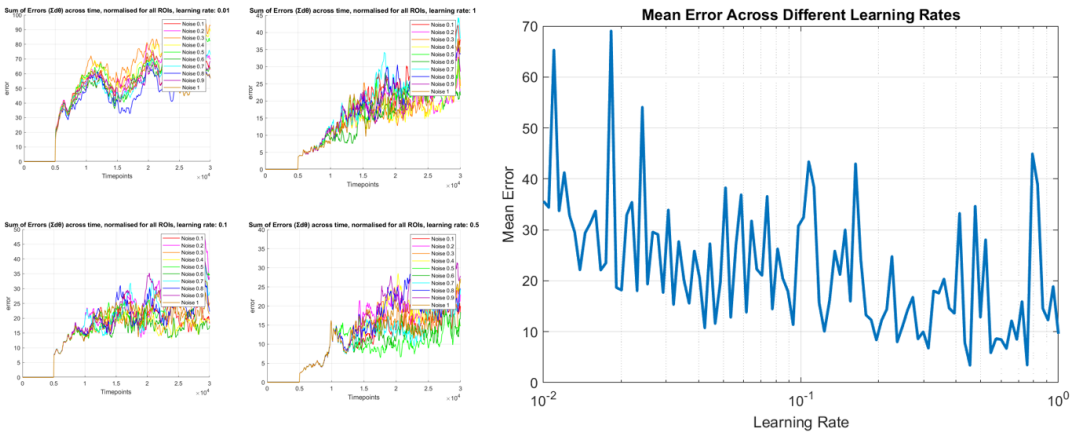


FIGURE 4.5: Kuramoto model: (a) Simulation errors over time for four instances of learning rate ($lr = 0.01$, $lr = 0.1$, $lr = 0.5$, and $lr = 1$), showing the impact of different learning rates on error progression under the Hebbian learning model- The introduction of learning increases variability compared to the scenario without learning. (b) Tuning the learning rate: illustrates how adjusting the learning rate impacts the overall network's behavior and error progression over time.

### 4.1.4 Izhikevich model

In this next part, we employed the Izhikevich model to simulate the neuronal dynamics focusing on the response of individual neurons to varying input currents.

Each region of interest (ROI) was modeled as a single neuron, allowing for detailed analysis of both the input current and membrane potential. Figure 4.1.4 (a) illustrates the input current and membrane potential over time. The membrane potential varied between approximately $-65\,\text{mV}$ and $+30\,\text{mV}$, reflecting the dynamic nature of neuronal activity in response to the oscillatory input. The oscillatory input significantly influenced the membrane potential, with clear peaks corresponding to the oscillation frequency. The neuron demonstrated the expected spiking behavior, as indicated by the rapid excursions of the membrane potential toward $+30\,\text{mV}$.

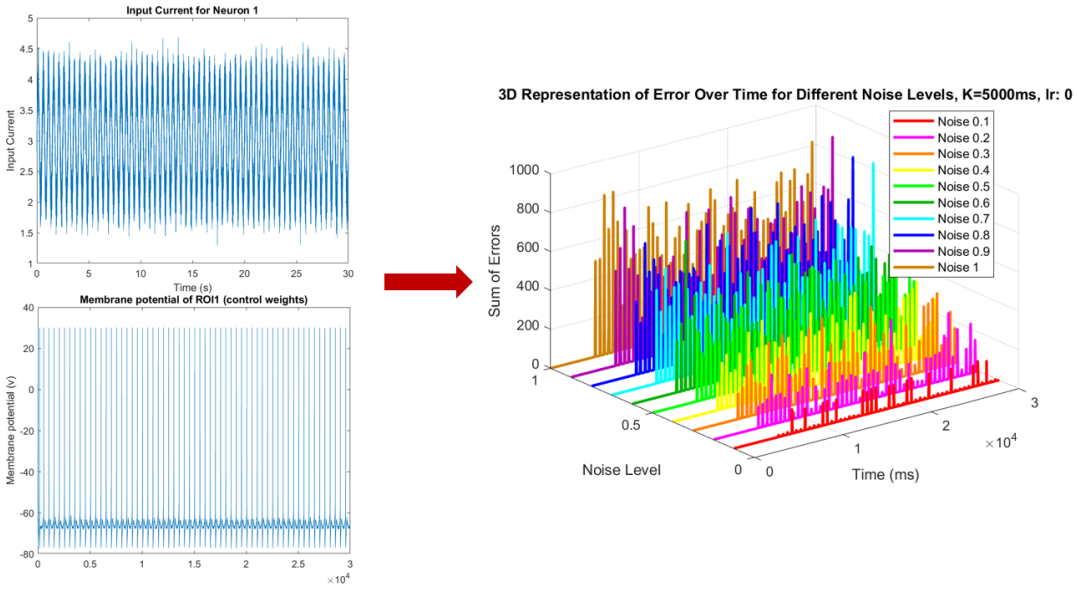


FIGURE 4.6: Dynamic behavior of the Izhikevich model illustrated across three panels: (a) The input current to neuron (ROI) 1, showcasing the oscillatory nature of the input that drives neuronal activity; (b) The membrane potential of ROI1 under control conditions, illustrating fluctuations in membrane potential as the neuron responds to the input current; (c) A 3D representation of error over time for different noise levels, with parameters set to $k = 5000$ ms and learning rate $lr = 0$, highlighting the impact of varying noise levels on the network's performance.

Figure 4.1.4 (c) shows the sum of errors $\Sigma\Delta\theta$ across time for different noise levels. As illustrated, there was a notable increase in error as noise levels increased. The sum of errors displayed a clear positive correlation with noise levels, suggesting

that higher noise levels lead to increased deviations in the neuron's output. Notably, the error for a noise level of 0.1 was significantly lower than that for a noise level of 1, indicating that noise has a detrimental effect on neuronal performance. With the introduction of even low noise levels (e.g., Noise 0.2 or Noise 0.4), errors begin to accumulate, especially in the later stages of the simulation, indicating sensitivity to noise perturbations. The error growth becomes more pronounced at higher noise levels (e.g., Noise 0.8, Noise 1), where spikes in error occur earlier in time, showing a strong disruption of the system's regularity.
The 3D representation highlighted distinct patterns in error across time and noise levels. The increase in error with rising noise levels was apparent, with certain timepoints showing sharper increases in error rates.
In the case of $k$ hyperparameter tuning, Figure 4.7 shows the mean error as a function of different $k$. The mean error fluctuates within a range of approximately 4.2 to 5.4. This variation suggests that the timing of noise introduction has a significant impact on the system's performance. However, despite this increased variability in error as $k$ progresses, the overall trend does not show a clear upward or downward bias, indicating that the sensitivity to noise may not have a linear relationship with the timepoint but may instead depend on the interaction of noise with specific internal dynamics at different phases.

However, when investigating the influence of different learning rates on error behavior under varying noise conditions, as modeled in the Izhikevich system, it was observed that as the learning rate decreases (from $lr = 1$ to $lr = 0.1$), the overall sum of errors tends to increase significantly. At $lr = 1$ ( 4.8 top right plot), the error remains relatively low across noise levels. While noise does cause fluctuations, the system exhibits robust performance even under higher noise levels. In contrast, at lower learning rates (e.g., $lr = 0.01$, 4.8 bottom left plot), the error grows considerably for all noise levels, with the system accumulating errors rapidly, particularly at higher noise levels (e.g., Noise 0.9, Noise 1.0). The transition from $lr = 0.5$ to $lr = 0.01$ demonstrates that higher learning rates allow the

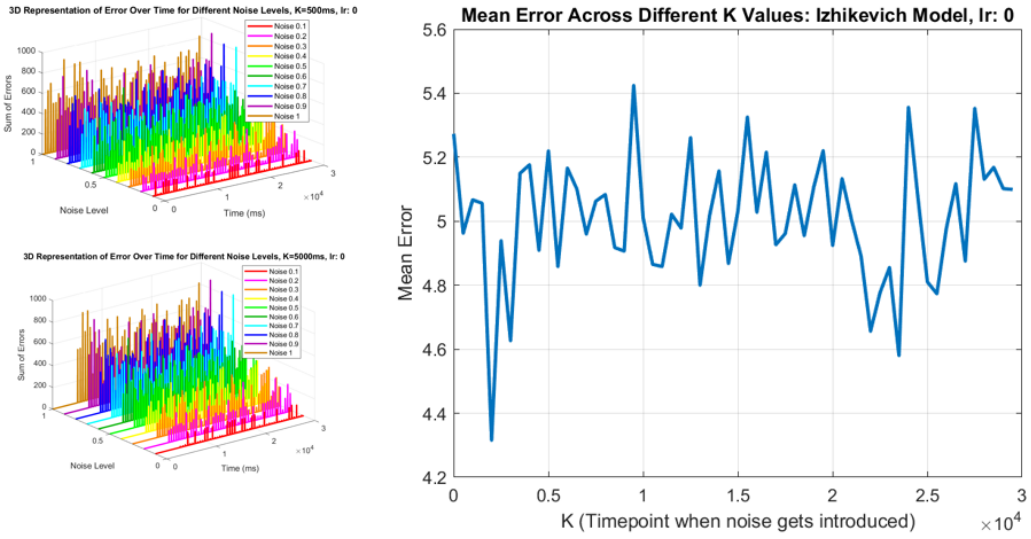


FIGURE 4.7: izhikevich Model: The impact of noise introduction timepoint $k$ on network dynamics. (a) The error progression over time for two different instances of $k$, $k = 5000ms$ and $k = 10000ms$ with $learningrate = 0$ (b) The mean error as a function of the $k$ hyperparameter.

system to adapt more effectively to noise perturbations, resulting in lower and more stable error values. Meanwhile, lower learning rates exacerbate the system's error accumulation over time, especially under high-noise conditions.
The plot on the rightside of 4.8 shows the mean error as a function of different learning rates. The mean error decreases sharply as the learning rate increases from 0 to 0.2, indicating that the system becomes significantly more accurate at higher learning rates. Beyond a learning rate of approximately 0.2, the mean error stabilizes at a very low value, suggesting that the system reaches an optimal learning rate range where further increases no longer contribute significantly to reducing the error. The system demonstrates its optimal performance at learning rates around 0.2, where the error is minimized and remains low despite variations in the noise levels.

We explored the influence of varying learning rates on the Izhikevich model's performance and its effect on the system's error. Notably, as the learning rate increased, the overall error between the noisy and control simulations steadily decreased, even reaching near-zero levels at the highest learning rates. This

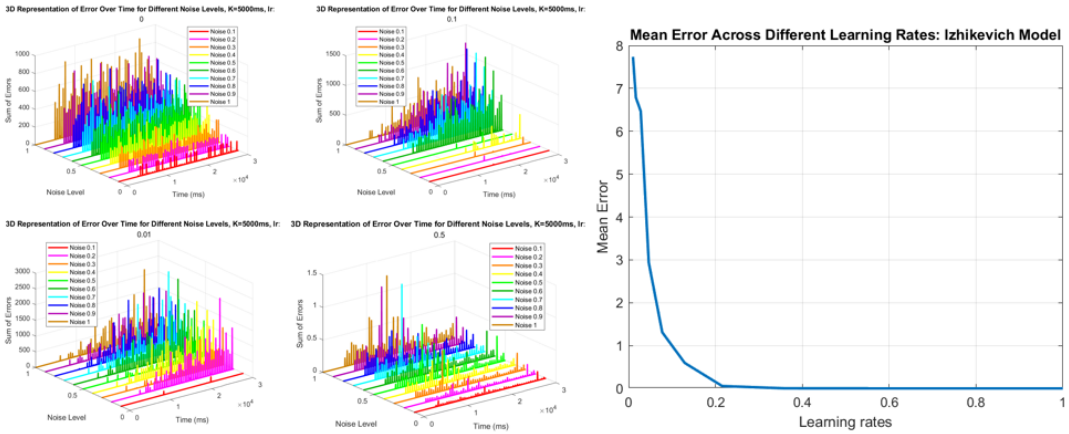


FIGURE 4.8: IZhikevich Model: (a) Simulation errors over time for four instances of learning rate ($lr = 0.01$, $lr = 0.1$, $lr = 0.5$, and $lr = 1$), showing the impact of different learning rates on error progression under the Hebbian learning model. (b) Tuning the learning rate: illustrates how adjusting the learning rate impacts the overall network's behavior and error progression over time.

behavior raised the concern that the system might be saturating, causing artificially low errors.

To investigate this further, we analyzed the activity of an individual neuron (neuron 1) for the largest learning rate. The membrane potential of neuron 1 was plotted over time to check for signs of saturation, such as constant spiking or flatlining of the potential. The plot revealed that neuron 1 maintained normal firing dynamics, with no indications of saturation (i.e., no uncharacteristic or constant behavior in the membrane potential). This finding suggests that the reduction in error is likely due to effective learning rather than an artifact of system saturation. The neurons continued to exhibit realistic spiking behavior, indicating that the learning process was functioning correctly, even at higher learning rates. Therefore, the results, showing a reduction in noise-induced errors, appear to be valid and reflective of actual system improvements.

## 4.2 Analysis of ROI contributions

The analysis of the contributions of ROIs revealed significant differences in how connectivity strength impacts the final error across the two simulation models, Kuramoto and Izhikevich.
The correlation coefficients obtained indicate the relationships between the connectivity strengths of the regions of interest (ROIs) and the final errors. The Kuramoto model exhibited a moderate positive relationship with a Spearman's coefficient of 0.3138. This suggests that, in this model, ROIs with higher connectivity strength tend to contribute slightly more to the final error. For example, ROIs such as ROI 11 *(lh.lateral_occipital)* and ROI 12 *(lh.lingual)* demonstrated higher strengths 4.9, which were associated with increased final error contributions. This observation indicates that these regions play a more significant role in the error dynamics of the Kuramoto model, reflecting a potential sensitivity to connectivity variations.
Conversely, the Izhikevich model demonstrated a strong negative relationship, as evidenced by a Spearman's coefficient of $-0.7704$. This indicates that in the Izhikevich framework, ROIs with higher connectivity strength actually contribute less to the errors. For instance, ROI 35 *(rh.thalamus)*, exemplified this trend by showing one of the strongest negative contributions to the final error, indicating that as its connectivity strength increased, the associated error decreased significantly. Additionally, regions like ROI 36 *(rh.caudate)* further supported this relationship by contributing less to errors as their connectivity increased.
Then, in order to gain a more comprehensive understanding of the contributions of different brain regions to the noise in the neural simulations, we clustered the ROIs based on their anatomical lobes. This clustering allowed us to analyze the spatial contributions of each lobe in both the Kuramoto and Izhikevich models.

| | Names | Lobe | Strengths | Kuramoto model, lr=0 | Izhikevich model, lr=0 |
|---|---|---|---|---|---|
| ROI 1 | lh.bankssts | Temporal | 5.5214 | 0.0106 | 0.0301 |
| ROI 2 | lh.caudala... | Frontal | 15.6500 | 0.0109 | 0.0204 |
| ROI 3 | lh.caudalm... | Frontal | 15.9607 | 0.0352 | 0.0139 |
| ROI 4 | lh.cuneus | Occipital | 27.1321 | 0.0094 | 0.0121 |
| ROI 5 | lh.entorhinal | Temporal | 24.6714 | 0.0281 | 0.0083 |
| ROI 6 | lh.fusiform | Temporal | 26.6286 | 0.0109 | 0.0126 |
| ROI 7 | lh.inferiorp... | Parietal | 23.1393 | 0.0203 | 0.0123 |
| ROI 8 | lh.inferiorte... | Temporal | 24.0250 | 0.0135 | 0.0066 |
| ROI 9 | lh.isthmus... | Parietal | 23.4000 | 0.0119 | 0.0118 |
| ROI10 | lh.lateraloc... | Occipital | 34.1357 | 0.0289 | 0.0038 |
| ROI11 | lh.lateralor... | Frontal | 24.4000 | 0.0059 | 0.0084 |
| ROI12 | lh.lingual | Occipital | 36.0321 | 0.0162 | 0.0058 |
| ROI13 | lh.medialor... | Frontal | 28.1964 | 0.0162 | 0.0068 |
| ROI14 | lh.middlete... | Temporal | 22.5607 | 0.0052 | 0.0091 |
| ROI15 | lh.parahipp... | Temporal | 17.6786 | 0.0109 | 0.0094 |
| ROI16 | lh.paracent... | Frontal | 15.8893 | 0.0259 | 0.0163 |
| ROI17 | lh.parsoper... | Frontal | 19.9286 | 0.0069 | 0.0153 |
| ROI18 | lh.parsorbit... | Frontal | 19.2536 | 0.0027 | 0.0134 |
| ROI19 | lh.parstrian... | Frontal | 23.0643 | 0.0211 | 0.0142 |
| ROI20 | lh.pericalca... | Occipital | 21.1464 | 0.0103 | 0.0105 |
| ROI21 | lh.postcent... | Parietal | 28.0286 | 0.0279 | 0.0075 |
| ROI22 | lh.posterior... | Parietal | 18.7071 | 0.0073 | 0.0089 |
| ROI23 | lh.precentral | Frontal | 29.1000 | 0.0043 | 0.0063 |
| ROI24 | lh.precuneus | Parietal | 42.4429 | 0.0047 | 0.0063 |
| ROI25 | lh.rostralan... | Frontal | 16.2286 | 0.0111 | 0.0070 |
| ROI26 | lh.rostralmi... | Frontal | 36.6000 | 0.0131 | 0.0122 |
| ROI27 | lh.superiorf... | Frontal | 50.8893 | 0.0409 | 0.0048 |
| ROI28 | lh.superior... | Parietal | 49.3393 | 0.0441 | 0.0046 |
| ROI29 | lh.superiort... | Temporal | 26.1857 | 0.0180 | 0.0117 |
| ROI30 | lh.suprama... | Parietal | 14.5107 | 0.0044 | 0.0150 |
| ROI31 | lh.frontalpole | Frontal | 15.5143 | 0.0029 | 0.0176 |
| ROI32 | lh.temporal... | Temporal | 26.8250 | 0.0093 | 0.0140 |
| ROI33 | lh.transver... | Temporal | 7.9250 | 0.0057 | 0.0225 |
| ROI34 | lh.insula | Insular | 26.8607 | 0.0253 | 0.0104 |
| ROI35 | lh.thalamus | Subcortical | 42.7786 | 0.0466 | 0.0055 |
| ROI36 | lh.caudate | Subcortical | 22.3000 | 0.0341 | 0.0086 |
| ROI37 | lh.putamen | Subcortical | 32.4643 | 0.0202 | 0.0064 |
| ROI38 | lh.pallidum | Subcortical | 25.5821 | 0.0154 | 0.0109 |
| ROI39 | rh.amygdala | Subcortical | 25.2286 | 0.0121 | 0.0110 |
| ROI40 | rh.hippoca... | Subcortical | 11.8679 | 0.0072 | 0.0245 |
| ROI41 | rh.accumb... | Subcortical | 14.6286 | 0.0026 | 0.0242 |
| ROI42 | rh.bankssts | Temporal | 6.7571 | 0.0012 | 0.0338 |
| ROI43 | rh.caudala... | Frontal | 14.5607 | 0.0012 | 0.0214 |
| ROI44 | rh.caudalm... | Frontal | 16.8857 | 0.0095 | 0.0120 |
| ROI45 | rh.cuneus | Occipital | 26.6143 | 0.0164 | 0.0141 |
| ROI46 | rh.entorhinal | Temporal | 23.7036 | 0.0028 | 0.0131 |
| ROI47 | rh.fusiform | Temporal | 26.8679 | 0.0034 | 0.0112 |
| ROI48 | rh.inferiorp... | Parietal | 23.8393 | 0.0015 | 0.0080 |
| ROI49 | rh.inferiorte... | Temporal | 25.0500 | 0.0061 | 0.0066 |
| ROI50 | rh.isthmus... | Parietal | 23.3714 | 0.0016 | 0.0116 |
| ROI51 | rh.lateraloc... | Occipital | 30.5750 | 0.0034 | 0.0068 |
| ROI52 | rh.lateralor... | Frontal | 22.7571 | 0.0067 | 0.0183 |
| ROI53 | rh.lingual | Occipital | 31.8429 | 0.0187 | 0.0085 |
| ROI54 | rh.medialor... | Frontal | 23.4179 | 0.0167 | 0.0127 |
| ROI55 | rh.middlete... | Temporal | 25.2464 | 0.0062 | 0.0065 |
| ROI56 | rh.parahipp... | Temporal | 20.3286 | 0.0010 | 0.0247 |
| ROI57 | rh.paracent... | Frontal | 16.1857 | 0.0075 | 0.0152 |
| ROI58 | rh.parsopa... | Frontal | 17.8571 | 0.0017 | 0.0080 |
| ROI59 | rh.parsorbit... | Frontal | 22.4571 | 0.0190 | 0.0091 |
| ROI60 | rh.parstrian... | Frontal | 25.3107 | 0.0055 | 0.0142 |
| ROI61 | rh.pericalc... | Occipital | 20.8571 | 0.0101 | 0.0164 |
| ROI62 | rh.postcent... | Parietal | 26.7679 | 0.0059 | 0.0075 |
| ROI63 | rh.posterior... | Parietal | 16.4036 | 0.0154 | 0.0137 |
| ROI64 | rh.precentral | Frontal | 28.1429 | 0.0020 | 0.0090 |
| ROI65 | rh.precune... | Parietal | 40.2679 | 0.0100 | 0.0095 |
| ROI66 | rh.rostralan... | Frontal | 15.4857 | 0.0029 | 0.0175 |
| ROI67 | rh.rostralmi... | Frontal | 39.5214 | 0.0053 | 0.0053 |
| ROI68 | rh.superiorf... | Frontal | 48.6250 | 0.0017 | 0.0055 |
| ROI69 | rh.superior... | Parietal | 48.5143 | 0.0137 | 0.0043 |
| ROI70 | rh.superiort... | Temporal | 26.3571 | 0.0131 | 0.0060 |
| ROI71 | rh.supram... | Parietal | 16.7679 | 0.0132 | 0.0146 |
| ROI72 | rh.frontalpole | Frontal | 20.9107 | 0.0135 | 0.0147 |
| ROI73 | rh.temporal... | Temporal | 24.2893 | 0.0077 | 0.0098 |
| ROI74 | rh.transver... | Temporal | 7.3071 | 0.0089 | 0.0195 |
| ROI75 | rh.insula | Insular | 29.9821 | 0.0309 | 0.0093 |
| ROI76 | rh.thalamus | Subcortical | 41.7964 | 0.0394 | 0.0040 |
| ROI77 | rh.caudate | Subcortical | 21.5929 | 0.0023 | 0.0212 |
| ROI78 | rh.putamen | Subcortical | 35.2393 | 0.0046 | 0.0090 |
| ROI79 | rh.pallidum | Subcortical | 26.8179 | 0.0033 | 0.0086 |
| ROI80 | rh.amygdala | Subcortical | 24.7214 | 0.0031 | 0.0160 |
| ROI81 | rh.hippoca... | Subcortical | 12.8929 | 0.0019 | 0.0197 |
| ROI82 | rh.accumb... | Subcortical | 16.2393 | 0.0027 | 0.0254 |

FIGURE 4.9: ROI contribution for Kuramoto model and Izhikevich model

In the Kuramoto model, as shown at Figure 4.10, the Frontal lobe emerged as the most influential, contributing approximately 29% to the overall noise. This dominance suggests that the Frontal lobe plays a critical role in the dynamics of the Kuramoto framework, may lead to greater fluctuations and, hence, more substantial contributions to the final error. The Subcortical areas followed closely, contributing about 20%, highlighting its significant involvement in the error dynamics. The Parietal lobe and Temporal lobe contributed 18% and 16%, respectively, indicating that even regions with lower connectivity can have notable effects on the overall error. The Insular Cortex, while smaller in total strength, still contributed about 6% and the Occipital Lobe indicated a total error contribution of 11%.

In contrast, the Izhikevich model demonstrated different dynamics. The Frontal lobe continued to be the leading contributor, accounting for 32% of the total noise, reaffirming its critical role across both models. However, the relative contributions of the other lobes shifted, with the Temporal lobe contributing 26%, and the Subcortical areas contributing 19%. The Occipital lobe showed a notable contribution of 8%, the Parietal 14%, while the Insular lobe had the smallest share at 2%. These shifts in contributions indicate that the error dynamics in the Izhikevich model might be influenced differently by each lobe, with higher contributions from the Subcortical regions compared to

the Kuramoto model.

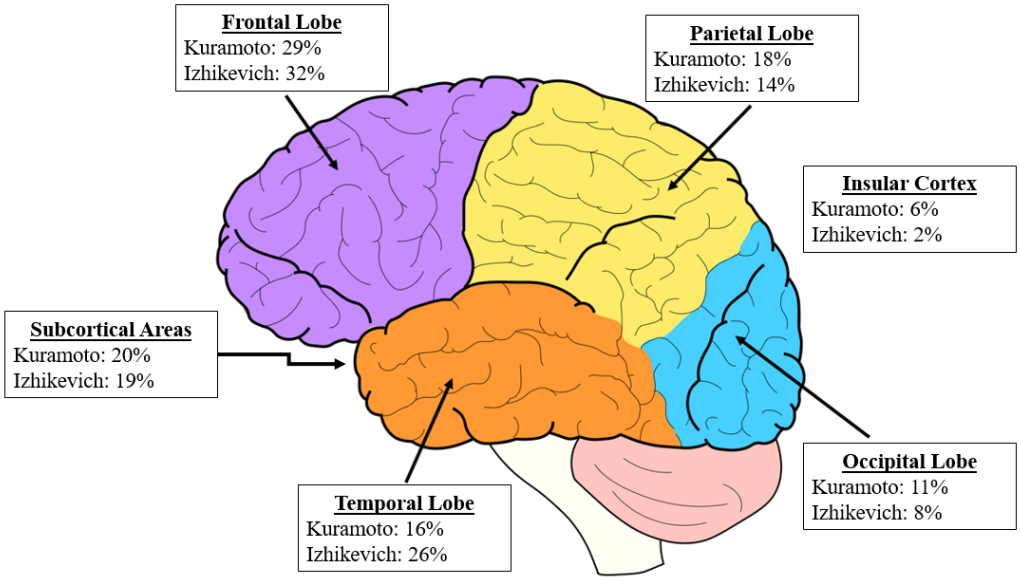


FIGURE 4.10: Spatial Contribution, clustered for each anatomical brain-area

# Chapter 5

# Discussion

Chapter 5. *Discussion*

## 5.1 Interpretation of results

### 5.1.1 Simulation of Results

The simulations in this study were divided into three distinct phases to effectively mimic the process of whole-brain emulation (WBE) and analyze the effects of noise on neural dynamics. The first phase represents the period prior to the introduction of noise, simulating the normal operation of a functioning brain in real-time. This phase serves as a baseline, reflecting how an individual's brain processes information under ideal, noise-free conditions.
The second phase marks the branching point where noise is introduced. This stage simulates the data acquisition process in the WBE scenario, where neural data is collected through imaging techniques. It is at this point that measurement errors, and the inherent noise-levels they introduce, become a factor. This phase essentially captures the transition from an error-free representation to one where inaccuracies begin to affect the data and the transition from the biological brain to the computational brain.
Finally, the third phase involves running two separate sets of simulations. The first set, based on the control data, represents how the computational brain-simulation would behave under ideal circumstances, where the imaging techniques produced no errors on the acquired data. The second set, using the noisy

data, simulates how the brain would operate in the computer-generated replica, with varying levels of noise that more realistically emerge from the experimental imaging procedures. This final phase allows for the direct comparison of brain activity under ideal conditions with the altered activity that results from the presence of noise, providing key insights into the impact of data acquisition errors on the fidelity of WBE simulations.

### 5.1.2 Model Performance

In both the Kuramoto and the Izhikevich models, a clear and consistent relationship was observed between the level of noise introduced into the system and the overall error in the model's output. The results suggest that the presence of noise during data collection is not merely a minor inconvenience but rather a key factor that substantially affects the accuracy of subsequent neural simulations.
As noise levels increase, their influence on the system's error also grows, ultimately impairing the model's ability to faithfully replicate neural behavior. This reinforces a central point: in brain emulation and computational neuroscience, controlling for and minimizing noise during data acquisition is absolutely essential. Even relatively small amounts of noise can have far-reaching effects, potentially distorting the later stages of the simulation and resulting in less accurate predictions or insights. The linkage between noise and total error observed in both models highlights the inherent sensitivity of simulations to initial data conditions. These findings underscore not only the importance of using precise and highly accurate measurement tools during the data acquisition phase, but also the need to explore additional strategies for mitigating or correcting these errors during the simulation process itself.

### 5.1.3 k Hyperparameter Tuning

Regarding the tuning of the hyperparameter k, our investigation aimed to explore the influence of varying k values across time,

particularly examining whether extending the pre-branching time period (before noise introduction) would help stabilize the system. The hypothesis was that a longer pre-branching period might condition the system, leading to more stable simulations afterward. This, in turn, could potentially influence the degree of difference observed between the control simulations and those based on noisy data.
However, the results showed irregular patterns in both the Kuramoto and Izhikevich models. There was no clear or consistent relationship between the value of k and the stability of the later simulations. In other words, increasing the pre-branching time did not consistently lead to better alignment between the control data and the noisy data, nor did it provide a clear indication that a longer pre-noise period would enhance the simulation's performance.
Interpreting this biologically, it is indeed plausible that these irregular patterns reflect the inherent complexity of brain function. In a biological brain, the ongoing processes are dynamic and ever-changing as the brain continuously integrates new information, adapts to its environment, and modifies its neural pathways based on experience and learning. This continuous flux could mean that no specific pre-conditioning period can fully stabilize brain activity, as the brain itself is constantly evolving and adjusting in real time. Even during a period, like our simulations, where external factors are controlled, the brain remains susceptible to internal fluctuations and novel stimuli may disrupt or change its activity.
Thus, the lack of a clear relationship between k and the simulation's stability may be a reflection of this biological reality. The brain is not a static system; it is highly adaptive and unpredictable, so any artificial pre-conditioning period is unlikely to "prepare" the brain in a way that leads to consistently better simulation outcomes. Instead, the results might suggest that the brain's intrinsic variability cannot be captured or stabilized simply by adjusting the time span before noise introduction. The simulations, like the brain, are inherently sensitive to new information and environmental changes, and this variability is a fundamental feature of neural dynamics.

### 5.1.4 Learning rate tuning

In the context of learning rate (lr) tuning, the differences between the Kuramoto and Izhikevich models offer intriguing insights. While the Kuramoto model showed no clear relationship between learning rate and noise, exhibiting an unpredictable and inconsistent pattern, the Izhikevich model displayed a steady reduction in noise as the learning rate increased. At a certain learning rate value, the noise levels even approached zero. This finding suggests that learning mechanisms, especially in more biologically detailed models like Izhikevich, may play a critical role in compensating for initial measurement errors. This observation is particularly significant for whole-brain emulation (WBE) efforts, where errors stemming from imperfect data acquisition could be rectified through learning dynamics embedded within the model itself.

However, it's important to acknowledge that large learning rates, although effective at reducing noise in this case, could also lead to system saturation or oversimplification of brain dynamics, where the model's flexibility to adapt to new or more complex environments is compromised. Such oversimplification would limit the model's ability to faithfully replicate real neural behavior, especially in the context of lifelong learning and adaptation, critical elements of brain function.

Thus, while the results from the Izhikevich model offer hope for reducing noise and correcting measurement errors, more research is needed to fully explore how learning rates affect system behavior over time. Particularly, biologically realistic models may offer the most promise, as internal brain mechanisms like synaptic plasticity are likely to naturally mitigate errors over time. This insight opens up the possibility that incorporating adaptive learning mechanisms into simulations could help overcome one of the key barriers holding back WBE: the issue of noise introduced during data acquisition.

### 5.1.5 Spatial Contribution

In the Kuramoto model, the differences in the relationships between connectivity strength and error in the two models, appeared to be moderate positive. ROIs with higher connectivity contributed more to the final error. This suggests that the Kuramoto model may be more sensitive to variations in connectivity, meaning that regions with stronger connections introduce greater fluctuations, increasing the overall error.
In practical terms, this implies that errors from data acquisition, particularly in regions of high connectivity strength, are amplified during simulation. Therefore, improving the precision of data acquisition in highly connected cortical areas—such as those identified in the analysis—could reduce error in Kuramoto-based simulations. Conversely, in the Izhikevich model, the strong negative correlation between connectivity and error suggests that higher connectivity regions reduce the error contribution. This pattern indicates that the Izhikevich model benefits from higher connectivity in certain areas, stabilizing the system and reducing noise. This model seems to capture a more nuanced biological behavior, where highly connected regions may play a stabilizing role in brain dynamics, decreasing error. This finding could be especially important for improving imaging setups, as it suggests that accurately capturing the connectivity of more weakly connected areas, might be crucial for reducing error in more biologically accurate models like Izhikevich.

## 5.2 Significance of findings

The results of this study provide critical insights into the dynamics of noise and error propagation in brain simulations, specifically within the Kuramoto and Izhikevich models, and highlight the importance of accurate data acquisition for whole-brain emulation (WBE). The findings emphasize that the impact of measurement error on simulation performance is significant and

cannot be overlooked in WBE research. While much of the existing work in the field focuses on the computational infrastructure required to host a brain model—such as processing power, memory capacity, and parallelization techniques—our study underscores the equally crucial role of addressing measurement error in the data acquisition phase.
This research highlights that the introduction of noise during the acquisition of neural data, such as through imaging techniques like fMRI or DTI, can profoundly affect the accuracy of simulations. Both models demonstrated a clear relationship between the level of noise and the resulting error, with certain brain regions or lobes contributing more significantly to error propagation. These results suggest that improving the resolution, precision, and consistency of imaging technologies is just as important as refining the computational algorithms or hardware that host these simulations. Without addressing the inaccuracies at the data acquisition stage, even the most advanced and biologically realistic models will be prone to significant error, limiting the potential of WBE.

## 5.3 Data Model limitations

While this study provides valuable insights into the effects of noise on whole-brain simulations, there are several limitations in both the data and the models employed that must be acknowledged. One of the key limitations is the relatively simplified nature of the models used—Kuramoto and Izhikevich. These models, while effective for certain types of neural simulation, do not fully capture the biological complexity of actual brain function. Both models abstract away many details of neural activity, such as the intricate interplay between different types of neurons (excitatory and inhibitory) and the various neurotransmitters and signaling pathways that regulate brain activity. This limitation stems partly from the computational resources available for this research, which constrained us to models that could run efficiently on more limited hardware. More biologically realistic models, like spiking neuron networks with

detailed synaptic plasticity, could have provided deeper insights but require far greater computational power.
Another limitation relates to the granularity of the regions of interest (ROIs). Each ROI represents a large and heterogeneous collection of neurons, encompassing potentially hundreds of thousands of different types of cells with unique firing patterns and functions. By reducing these vast regions to single units in the models, we are inherently oversimplifying the actual neural dynamics at play. This aggregation of neurons makes it impossible to capture the full diversity of neural responses to noise and could mask important sub-regional variations in how errors propagate through the brain. This limitation highlights the need for more refined, high-resolution models that can account for the differences within and between brain regions.

# Chapter 6

# Conclusions and future work



## 6.1 Summary of key findings

This study explored the impact of noise on brain simulations using both the Kuramoto and Izhikevich models, focusing on how measurement error affects WBE. A clear link between noise and the total error emerged, highlighting that even small inaccuracies in data acquisition can significantly impact neural simulations. Specifically, higher noise levels correlated with greater errors, affirming that precision in data gathering is crucial for accurate WBE.

Our analysis of the Regions of Interest (ROIs) showed that connectivity strength has varying effects depending on the model. In the Kuramoto model, stronger connectivity in ROIs was associated with greater error contributions, while the Izhikevich model exhibited an inverse relationship, suggesting a more complex dynamic between connectivity and error in more biologically realistic simulations. The clustering of ROIs into anatomical lobes further revealed the Frontal lobe as a critical region, influencing noise contributions in both models, though differed for the rest of the anatomical regions.

Additionally, parameter tuning for the learning rate in the Izhikevich model revealed a trend where increasing the learning rate reduced the noise and brought it close to zero at higher values. This finding suggests the potential to correct measurement errors through learning mechanisms, in biologically accurate models, offering a promising direction for mitigating inaccuracies in future WBE implementations. However, caution

must be exercised as higher learning rates may lead to system saturation, requiring further investigation.

These findings underscore the complexity of simulating brain activity and the importance of precise data acquisition methods to ensure reliable outcomes in WBE, while also opening up future avenues for improving the biological realism of such simulations.

## 6.2 Recommendations for future research

Future research in Whole Brain Emulation (WBE) should place greater emphasis on improving both data acquisition methods and simulation accuracy. Enhancements are needed not only in the hardware and imaging tools to capture more precise data but also in the preprocessing techniques to better handle and reduce measurement errors and also during the actual simulations. Current research tends to prioritize computational aspects, which are undoubtedly important, but the integrity of the input data remains equally critical. By refining both ends —data collection and model accuracy— WBE simulations can become far more reliable.

Additionally, there is a need for models that better capture the biological complexity of the brain. In our work, we have initiated efforts to simulate ROIs with 200 neurons, incorporating both excitatory and inhibitory activity. These advancements move us closer to accurate neural simulations and show promise for further reducing measurement error. This approach highlights how the biological realism of models can complement computational power in producing more faithful emulations.

The potential of WBE, especially in fields like artificial intelligence, neuroscience, and medicine, makes this an area of immense future relevance. Striking the right balance between computational power and data quality will be essential to achieving meaningful progress in brain emulation efforts.

# Bibliography


[1] Terrence J Sejnowski, Christof Koch, and Patricia S Churchland. "Computational neuroscience". In: *Science* 241.4871 (1988), pp. 1299–1306.

[2] Eric Mandelbaum. "Everything and more: The prospects of whole brain emulation". In: (2022).

[3] Gualtiero Piccinini. "Computationalism in the Philosophy of Mind". In: *Philosophy Compass* 4.3 (2009), pp. 515–532.

[4] Olaf Sporns. "The human connectome: origins and challenges". In: *Neuroimage* 80 (2013), pp. 53–61.

[5] Evan Weiss, Michael Kann, and Qi Wang. "Neuromodulation of neural oscillations in health and disease". In: *Biology* 12.3 (2023), p. 371.

[6] Rommy Von Bernhardi, Laura Eugen3́ın-von Bernhardi, and Jaime Eugenín. "What is neural plasticity?" In: *The plastic brain* (2017), pp. 1–15.

[7] John D Griffiths, Sorenza P Bastiaens, and Neda Kaboodvand. "Whole-brain modelling: past, present, and future". In: *Computational Modelling of the Brain: Modelling Approaches to Cells, Circuits and Networks*. Springer, 2021, pp. 313–355.

[8] Michael Marsalli. "Mcculloch-pitts neurons". In: *The 2008 Annual Meeting of the consortium on cognitive science instruction (ccsi)*. Vol. 1161. 2006, p. 1162.

[9] Mark Nelson and John Rinzel. "The hodgkin-huxley model". In: *The book of genesis* 2 (1995).

[10] Henry Markram. "The blue brain project". In: *Nature reviews neuroscience* 7.2 (2006), pp. 153–160.

[11] Henry Markram. "The human brain project". In: *Scientific American* 306.6 (2012), pp. 50–55.

[12] Matthew F Glasser et al. "The human connectome project's neuroimaging approach". In: *Nature neuroscience* 19.9 (2016), pp. 1175–1187.

[13] Hugo De Garis et al. "A world survey of artificial brain projects, Part I: Large-scale brain simulations". In: *Neurocomputing* 74.1-3 (2010), pp. 3–29.

[14] Lee Friedman, Gary H Glover, Fbirn Consortium, et al. "Reducing interscanner variability of activation in a multicenter fMRI study: controlling for signal-to-fluctuation-noise-ratio (SFNR) differences". In: *Neuroimage* 33.2 (2006), pp. 471–481.

[15] Ahmad Chaddad et al. "Electroencephalography signal processing: A comprehensive review and analysis of methods and techniques". In: *Sensors* 23.14 (2023), p. 6434.

[16] Congzhong Sun and Chaozhou Mou. "Survey on the research direction of EEG-based signal processing". In: *Frontiers in Neuroscience* 17 (2023), p. 1203059.

[17] Derek K Jones and Mara Cercignani. "Twenty-five pitfalls in the analysis of diffusion MRI data". In: *NMR in Biomedicine* 23.7 (2010), pp. 803–820.

[18] Krzysztof Gorgolewski et al. "Reproducibility in functional MRI: validation, improvement and future". In: ().

[19] Juan A Acebrón et al. "The Kuramoto model: A simple paradigm for synchronization phenomena". In: *Reviews of modern physics* 77.1 (2005), pp. 137–185.

[20] Peter Ashwin, Stephen Coombes, and Rachel Nicks. "Mathematical frameworks for oscillatory network dynamics in neuroscience". In: *The Journal of Mathematical Neuroscience* 6 (2016), pp. 1–92.

[21] Eugene M Izhikevich. "Which model to use for cortical spiking neurons?" In: *IEEE transactions on neural networks* 15.5 (2004), pp. 1063–1070.

[22] David C Van Essen et al. "The Human Connectome Project: a data acquisition perspective". In: *Neuroimage* 62.4 (2012), pp. 2222–2231.

[23] Huanjie Li et al. "Denoising scanner effects from multimodal MRI data using linked independent component analysis". In: *Neuroimage* 208 (2020), p. 116388.

[24] Laurena Holleran et al. "Axonal disruption in white matter underlying cortical sulcus tau pathology in chronic traumatic encephalopathy". In: *Acta neuropathologica* 133 (2017), pp. 367–380.

[25] Alex Fornito, Andrew Zalesky, and Edward Bullmore. *Fundamentals of brain network analysis*. Academic press, 2016.

[26] Mingrui Xia, Jinhui Wang, and Yong He. "BrainNet Viewer: a network visualization tool for human brain connectomics". In: *PloS one* 8.7 (2013), e68910.